STRAIN-INDUCING MECHANISM OF A ROLLING NIP ON A PAPER STACK

by

K. Ärölä and R. von Hertzen
Helsinki University of Technology
FINLAND

ABSTRACT

The rolling of a cylindrical drum on a stack of separate paper sheets is studied using the finite element method. A two dimensional model under plane strain conditions is considered. The material of the sheets is modeled by a linearly elastic orthotropic constitutive law. The friction between the various contacting surfaces is modeled by the conventional Coulomb's law. As a result of the FEM-calculations the time development of the displacements, stresses and strains of the paper layers is obtained. The slip behavior at the various contacting surfaces is presented. The results indicate the existence of an instant center in the stack demonstrated earlier experimentally. The micro-slip pattern of the contacting surfaces in the nip area and, particularly, at the trailing edge of the nip, seems to be the main reason for the tightening effect of the nip. The results are compared to the corresponding results for a solid elastic block under the rolling cylinder.

NOMENCLATURE

a	nip half-width
δ	vertical displacement of drum center
E_{ijkl}	component of elasticity tensor
ϵ_{ij}	strain component
γ_{ij}	shearing strain
p	contact pressure
q	contact shear stress
σ_{ij}	stress component
u	displacement
v	velocity

INTRODUCTION

Web transport between nipped rolls is common in many industrial processes dealing with paper, plastic, metal foils and textiles. The thin web is transported in rolling contact between two deformable axisymmetric bodies. Also, reeling and winding of thin webs is usually performed against a rotating drum creating a nip rolling over the web layers. The rolling nip removes the boundary layer of air following the web surface and increases the tension of the web passing the nip. The control of this tension increase is of primary importance when improving the roll structure in terms of optimal internal stresses and strains. Rolling contact phenomena including thin webs constitute a challenging problem, as they involve contact of different deformable bodies, free and loaded boundaries with a priori unknown borders, slip-and-stick patterns related to frictional behaviour, and geometric and possible material nonlinearities. Bentall and Johnson [1] considered an elastic strip passing between identical rollers. Their results provided details of the contact stresses and deformations, the indentation of the strip by the rollers, the contact width, and the speed at which the strip passes through the nip. No net tractive force was transmitted in the process. In their numerical solution they approximated the surface stress distribution by overlapping triangular elements. Soong and Li [2] studied the steady rolling contact with friction of two freely rolling dissimilar cylinders covered by bonded elastic layers and driving a thin sheet in the nip. The sheet was incompressible in its thickness, had extensional elasticity but no bending stiffness. They obtained the stresses and deformations as well as surface speeds for the cylinders and the sheet in a series form using a stress function formulation. Later Soong and Li [3] accounted for a pushing or pulling force acting at the tail end of the sheet. They studied the effect of the normal load and tail force on the speed ratios of the two cylinders and the sheet, and also the slippage and shear stress in the contact arc. The equations were solved by the collocation method and an iterative procedure. In both papers Soong and Li restricted their treatment to an isotropic elastic material. Batra [4] developed a finite element solution for the plane strain problem of a rubber covered roll indented by a rigid roll. Later Hinge and Maniatty [5] extended the finite element solution to the problem of steady rolling contact between rubber-layered rolls with thin media in the nip. The contact interface was assumed to be largely in stick and the bearing in the lower roll offered a negligible resisting torque. They also restricted to an isotropic elastic material law and the thin media was assumed to be inextensible, implying a constant thin media velocity through the nip. Kalker [6] considered the rolling contact of two parallel rigid cylinders covered with a number of homogeneous, isotropic and linearly elastic or viscoelastic layers. The layers were completely bonded to each other and to the cylinders so that no interlayer slippage could occur. Partial or complete slip could occur in the interface between the top layers of the cylinders. Friction was assumed to behave according to Coulomb's law with a constant friction coefficient. Kalker presented a fast method for the calculation of the elastic field on and inside the multilayered cylinders. A landmark investigation of the effect of a rolling nip upon a pile of separate layers was performed by Pfeiffer [7]. He reported experimental results on the strain-inducing mechanism of a rolling nip on a paper stack. This simulated the winding of a roll with an infinite radius. He observed in his experiment that the sheets nearest the stack surface were moved in the direction of the rolling nip

while sheets deeper in the stack moved in the opposite direction. He concluded that somewhere beneath the contact interface there must be an instantaneous center of rotation. In this paper, the first quantitative data displaying the effect of nip load, drum diameter, and the number of sheets in the stack on the amount of nip induced tension was presented. Pfeiffer's observations, however, accounted for external nip behaviour only and neither stress or strain distributions nor slip-stick patterns within the nip interface were considered. Good and Wu [8] considered the mechanism by which a nip roller can increase the wound-in tension in the outer layer of a wound roll. In their finite element analysis a Hertzian pressure distribution moved across the upper surface of the web while the lower web boundary was horizontally restrained by friction to accommodate slippage. They concluded that although the classical Hertzian contact stresses are always compressive throughout much of the depth of the web, they result in an elongating machine direction strain. As this elongating strain advances with the moving nip roll, web material attempts to advance in front of the nip and contact in towards the nip in back of the rolling nip. If the web material in back of the nip is constrained, a net increase in tension will result. Although Good and Wu provide the first basic understanding of the elongating strain in machine direction, their model comprises only one web layer and does not properly account for the rolling contact with friction since they employ a classical Hertzian pressure distribution with no shear stress at the upper surface of the web. Mc Donald and Menard [9] studied roll defects associated with interlayer movement experimentally. They considered, in particular, the formation of crepe wrinkles during reeling and winding. Crepe wrinkles consist of one or more folds of paper in the machine direction, and appear to be a consequence of layer-to-layer movement, quantified by means of J-lines, and out-of-plane buckling under in-plane compressive forces. They concluded that below the immediate surface layers the drum rolling against the conformable paper roll generated shear forces that caused the paper layers to slip, and the balance between the shear stress and frictional stress determined the amount of slippage and magnitude of the J-line. In their paper they gave several experimental results of the effect of drum diameter, cover material, frictional and radial compressive stress, and nip load on the size of the J-line. Recently, a rigorous contact mechanical model of the winding nip was presented by Jorkama and von Hertzen [10, 11]. Their model consisted of the wound roll, winding drum and the intervening sheet. The roll and drum were modeled as linearly elastic, orthotropic, homogeneous cylinders with a rigid core, and the sheet was modeled as an orthotropic material as well. In their numerical solution they utilized an iterative scheme, the Panagiotopoulos process, in an extended form for the solution of the stick-and-slip zones within the contact area. They presented a novel stick-and-slip mechanism, which explained the generation of the nip induced tension in the incoming sheet. They also properly described the conditions of the incoming sheet after the nip, which is a distinctive feature of winding compared to calendering. They utilized, however, a solid elastic model for the wound roll. The real layered structure of the roll with possible interlayer slippage can lead to a significantly different strain behaviour, especially in the vicinity of the nip.

In the present paper the layered structure of the paper stack is fully accounted for. The stresses, strains and displacements due to a rolling nip are calculated and the slip-and-stick behaviour at all contacting surfaces is presented. A detailed description of the interlayer movement of the paper sheets is given, and the mechanism

of the nip induced tension as a result of the shear stresses and opposing frictional forces is identified. The system studied here is very close to that used by Pfeiffer [7] in his experiment.

NUMERICAL RESULTS FOR A LAYERED STACK

Model Setup

Let us consider a cylindrical steel drum rolling with a velocity v to the right on a stack of ten paper sheets clamped at the left end as shown in Fig. 1. The sheets are placed on a steel surface at rest. If the situation is observed from a coordinate system translating with the center of the drum, the steel surface and the clamp bar are moving with the velocity v to the left and the drum is at rest (see Fig. 1). To

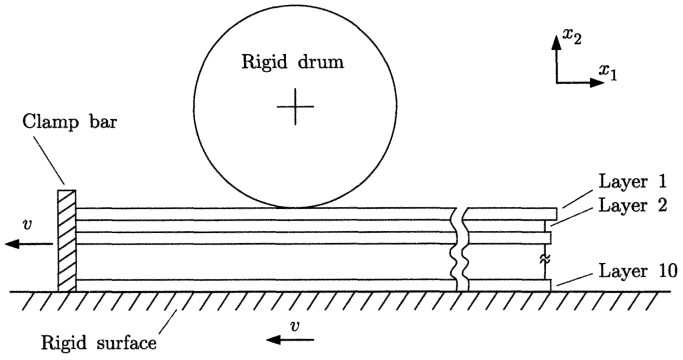

Figure 1: Drum rolling on a paper stack.

get a basic understanding of the phenomena and to keep the computational cost reasonable, a 2D-case under plane strain conditions is considered. Since the deformations of the steel drum and bottom plate are negligible compared to those of the paper sheets, the drum and plate are modeled as rigid. The paper sheets are modeled using four-noded plane strain finite elements[1]. A linear orthotropic constitutive model of the form

$$\begin{Bmatrix} \sigma_{11} \\ \sigma_{22} \\ \sigma_{33} \\ \sigma_{12} \\ \sigma_{13} \\ \sigma_{23} \end{Bmatrix} = \begin{bmatrix} E_{1111} & E_{1122} & E_{1133} & 0 & 0 & 0 \\ & E_{2222} & E_{2233} & 0 & 0 & 0 \\ & & E_{3333} & 0 & 0 & 0 \\ & & & E_{1212} & 0 & 0 \\ & & & & E_{1313} & 0 \\ & & & & & E_{2323} \end{bmatrix} \begin{Bmatrix} \epsilon_{11} \\ \epsilon_{22} \\ \epsilon_{33} \\ \gamma_{12} \\ \gamma_{13} \\ \gamma_{23} \end{Bmatrix} \tag{1}$$

is used. The x_1-axis is oriented in the sheet length, x_2-axis in the layer thickness and x_3-axis in the transverse direction. The friction between all contacting surfaces is modeled using Coulomb's friction law with a constant coefficient of friction.

At the beginning of the simulation the drum is touching the topmost paper layer at one point without any compressive forces. Then the vertical displacement δ of the

[1]ABAQUS/Explicit element type CPE4R

center of the drum is given as a time dependent kinematic condition and the drum is moved downward to generate a nip. After that the rolling process is activated by moving the bottom surface and the clamp bar to the left with a velocity v. One could also fix the bottom plate and the clamp bar and move the drum to the right. The former approach is preferred here due to an easier post processing of the results. To minimize the oscillatory effects caused by sudden changes in the displacement and velocity, the kinematic conditions are applied smoothly. The applied displacement and velocity are shown in Fig. 2 as a function of time. The values of the parameters

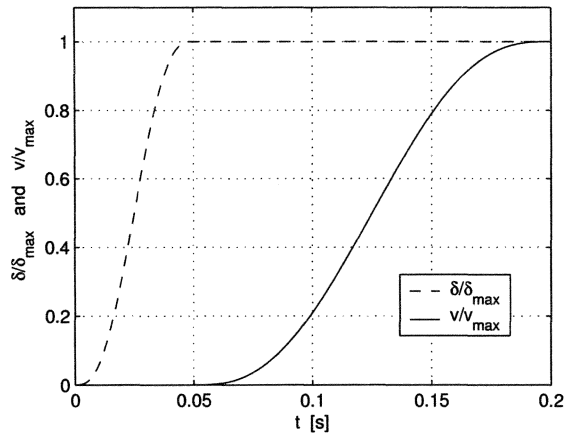

Figure 2: Time dependence of the vertical displacement of the drum and horizontal velocity of the clamp bar and bottom plate. After 0.2 s the values of the displacement and velocity are held constant.

and other data used in the calculations are given in the Appendix. The model had approximately 140000 degrees of freedom and the calculations were performed using the ABAQUS/Explicit computer code.

Development of the Sheet Tension

The time development of the tensile stress σ_{11} of the paper layers due to the rolling nip is shown in Fig. 3(a). All the stresses are calculated at the left end of the sheets. The curves show the evolution of the average stress in each individual layer. After an initial transient the tension of each individual layer rapidly tends towards a limit value as can be seen in Fig. 3(a). Similar experimental results concerning a nip roller on an aluminum strip were reported by Good and Wu [8] who found an exponential saturation of the strip tension with respect to the distance rolled. The final tensile stress distribution through the paper stack (at time $t = 0.7\,\mathrm{s}$) is shown in Fig. 3(b). The largest increase in tension takes place in the topmost layer. The tension then decreases layer by layer so that the fourth layer actually exhibits a compressive stress. The compressive stress is at largest in the sixth layer, whereas a small tensile stress is again found in the bottom layer. Note that the stress across each individual layer is constant as can be seen from Fig. 3(b).

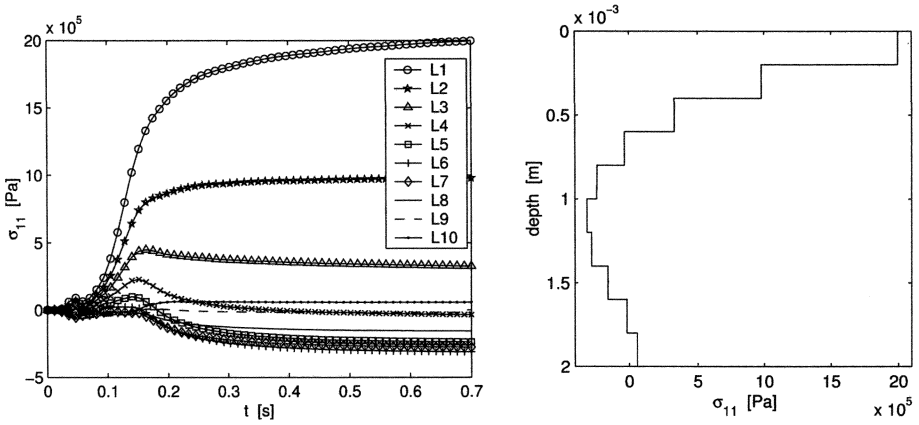

Figure 3: (a) Time development of the tensile stress of the paper layers L1,...,L10 due to the rolling nip. (b) The final tensile stress distribution through the paper stack. The stresses are calculated at the clamp bar.

Stresses in the Nip Area

A lot can be learnt about the events taking place in the nip by studying the stress distributions under the nip. In the following the tensile stresses σ_{11} and the contact shear stresses q of the sheets are considered. In the case of tensile stresses positive and negative signs indicate tension and compression, respectively. For the contact shear stresses the positive directions are shown in Fig. 4(a). Note that the

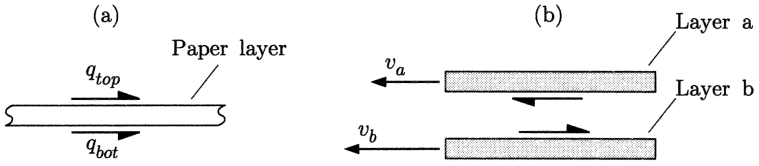

Figure 4: (a) Sign convention for the contact shear stresses q shown at the top and bottom of the layer. (b) The direction of the shear stresses reveals the slip direction.

direction of the shear stresses indicates the slip direction between the layers. If, for example, in Fig. 4(b) layer b is moving faster to the left than layer a, i.e. $v_b > v_a$, the real directions of the shear stresses are as shown in the figure. By the sign convention of Fig. 4(a) the shear stress on the bottom of layer a would be negative and on the top of layer b positive.

The tensile stresses in the sheets in the nip area are shown in Fig. 5. The solid line represents the average tensile stress, whereas the dashed and dashed-dotted lines show the tensile stress at the top and bottom of the layer, respectively. The x-coordinate is scaled by the nip half width a (= 6.752 mm). Consequently, the nip spans from $x/a = -1$ to 1. As can be seen, in the topmost layers most of the tightening action appears near the trailing edge of the nip. The tensile stress at

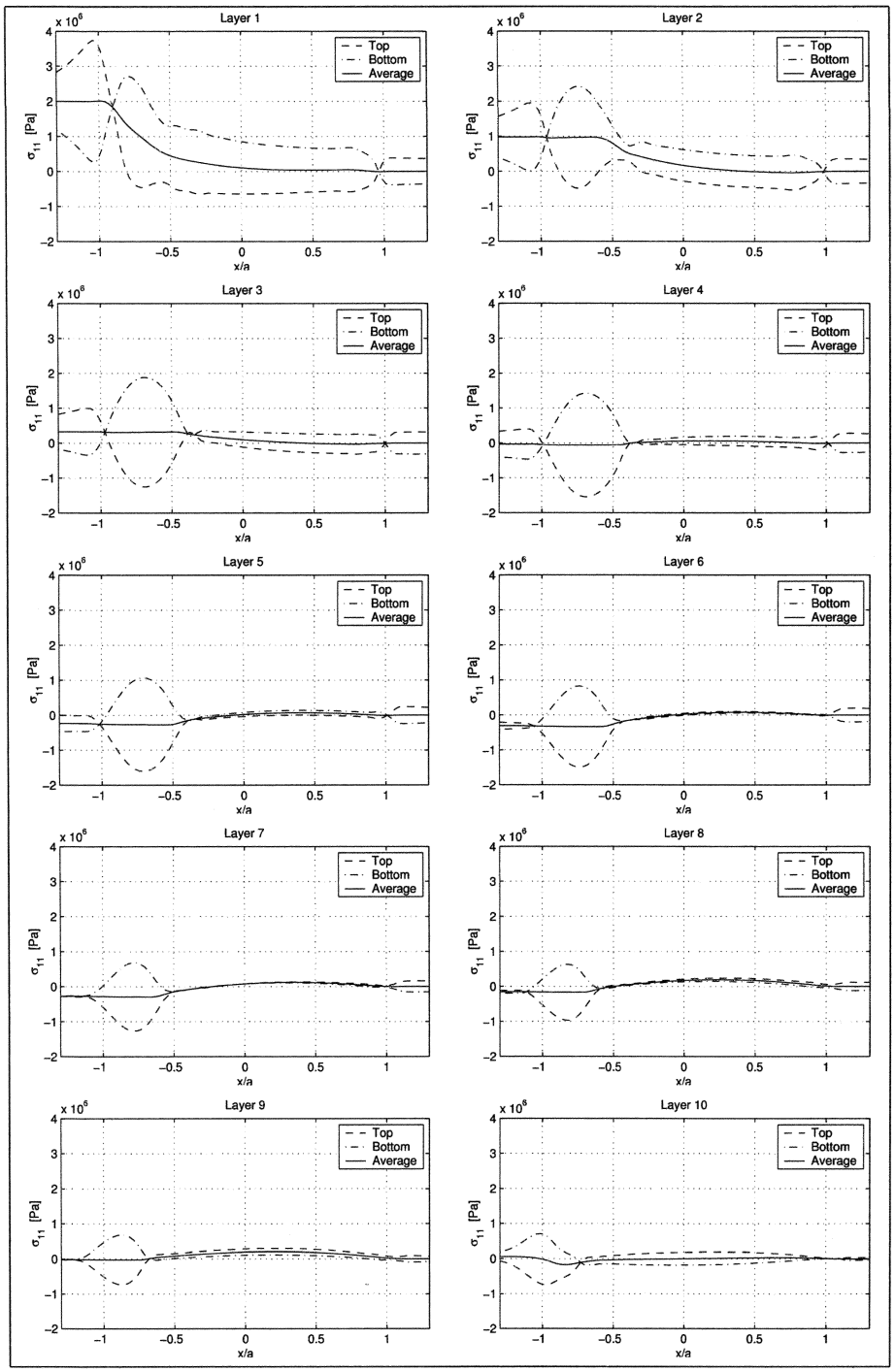

Figure 5: Tensile stress σ_{11} for each layer within the nip. The average, top and bottom stresses of the sheet are shown (solid, dashed and dashed-dotted lines, respectively).

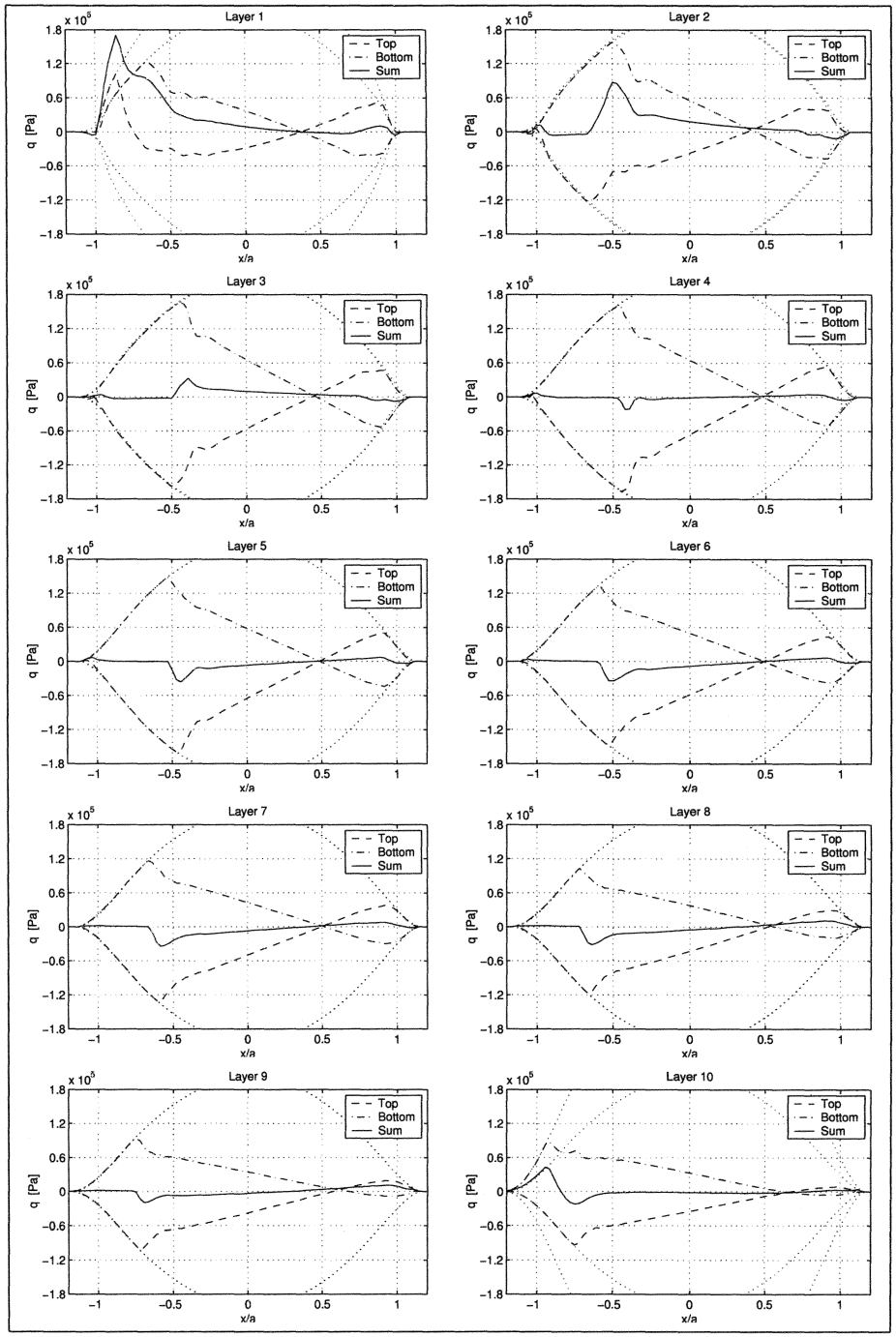

Figure 6: Contact shear stresses at the top and bottom surfaces of the layers (dashed and dashed-dotted lines, respectively) and the net shear stress (solid line). The friction limits are shown as dotted lines.

the top and bottom surface of a layer can differ considerably in the nip area. This difference is mainly due to the bending of the sheet under the drum. Behind the nip the tensile stress across each layer becomes constant very soon. Note that only the three layers on the top of the stack and the bottom layer are tightened and that the top layer is tightened by far most.

The contact shear stress distributions in the nip area for each layer are shown in Fig. 6. The dashed and dashed-dotted lines show the shear stress at the top and bottom surface of the layer, respectively. The solid line is the sum of the top and bottom stresses, i.e., the net shear stress on the sheet. To observe the areas of slip, the maximum and minimum values of the contact shear stress, that is the lines $q = \pm\mu p$ (p is contact pressure), are shown as dotted lines. If the shear stress falls on these lines, the contact is slipping. By inspecting the contact shear stress distributions we can draw several conclusions concerning the events taking place in the nip. Let us first examine the top surface of the first layer. In the vicinity of the leading edge of the nip the shear stress is positive (Fig. 6(a), dashed line) and the contact is slipping. The positive sign of the contact shear stress indicates that the top surface of the paper sheet is moving faster to the left than the surface of the drum. The center part of the contact zone is in a state of stick so that the drum and paper sheet have equal surface velocities. There is another slip zone near the trailing edge of the nip. The sign of the shear stress shows that again the surface of the sheet is moving faster than the drum. Let us then examine the shear stress at the bottom of the first layer (Fig. 6(a), dashed-dotted line). There is again a slip zone at the leading edge of the nip. Since the shear stress is negative, the bottom surface of the first layer is moving slower than the top surface of the second layer. Within the stick zone in the middle part of the nip, the shear stress becomes positive and finally rises to the upper friction limit. From here to the end of the nip sliding again occurs. Since the shear stress is positive, the bottom of the top layer is moving faster than the top of the second layer. Within about the first three quarters of the nip the shear stresses on the top and bottom surfaces of the first layer act in opposite directions and thus try to cancel each other. For this reason practically no tightening is observed in this part of the nip (see Figs. 5(a) and 6(a)). Near the trailing edge of the nip both shear stresses are positive so that they act additively, in the same direction. The force balance of the top layer requires that the effect of the shear stresses must be compensated for by the tensile stress. Consequently, a large increase in the tensile stress of the top layer occurs (see Fig. 5(a)).

Let us next consider the second paper layer. By inspection of the shear stresses (Fig. 6(b)) the following conclusions can be drawn. Within the slip zone near the leading edge of the nip the top of the second layer moves faster than the bottom of the first layer, while the bottom of the second layer moves slower than the top of the third layer. Within the other slip zone near the trailing edge of the nip the situation reverses. Note that the shear stresses are of opposite sign partially canceling each other throughout the nip. However, the net shear stress on the second layer still remains positive for most part of the nip so that some tightening in that layer occurs (see Figs. 5(b) and 6(b)).

In the third, fourth, ..., and ninth layers the shear stress behavior is qualitatively similar to that of the second layer except that below the third layer the net shear stress may become negative. In the tenth layer the net shear stress is slightly positive (see Figs. 6(c)–(j)). In conclusion, there are in every layer two slip zones near the

edges of the nip. Within the first one, at the leading edge of the nip, the upper layer (or drum) is moving slower than the layer below. Within the second one, near the trailing edge of the nip, the upper layer is moving faster than the layer below. Within the second slip zone, however, the top layer behaves in a unique manner as it also moves faster than the drum above. As already pointed out above, this phenomenon is essential in the tightening mechanism of a rolling nip.

It is instructive to have a look at the surface speeds within the contacts. The speeds are calculated from the surface strains and shear stresses. Some wavy behaviour due to a limited numerical accuracy has been filtered out from the figures. Fig. 7(a) shows the relative speed difference between the top surface of the first layer and the drum surface. At the beginning of the nip the speed difference is negative so that the surface of the top layer is moving faster than the drum surface resulting in a slip zone. This slip zone was already observed from the shear stress distribution of Fig. 6(a). A corresponding slip zone at the leading edge of the contact is not found in a typical capstan where the belt or sheet would be in a state of stick immediately at the beginning of the contact. The difference is due to the surface strains of the first layer in front of the nip caused by the bending of that layer as it approaches the nip region and due to the compressive strains experienced by this first layer under the drum at the beginning of the nip. This can be seen from Fig. 8 which shows the

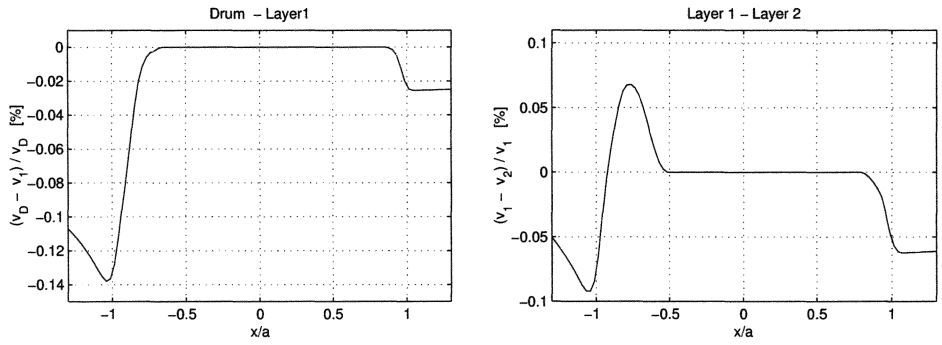

Figure 7: (a) Relative speed difference between the top surface of the first layer and the drum surface, and (b) between the bottom surface of the first layer and top surface of the second layer. Positive values indicate that the upper surface moves faster (to the left).

top and bottom surface strains and the vertical deflection of the first paper layer in the vicinity of the nip. Note the change of curvature of the first layer when it comes into contact with the rigid drum accompanied with a rapid decrease of the tensile strain at the top of the layer.

At $x/a \approx 0.8$ the relative speed difference goes to zero resulting in a stick zone (see Fig. 7(a)). This is maintained until the back of the nip where the contact starts slipping again. From $x/a \approx -0.7$ on the velocity of the first layer increases rapidly and the layer shoots out of the nip.

The relative speed difference between the bottom surface of the first layer and top surface of the second layer is shown in Fig. 7(b). The behaviour in the layers below is qualitatively similar, only the absolute values exhibit a decreasing trend.

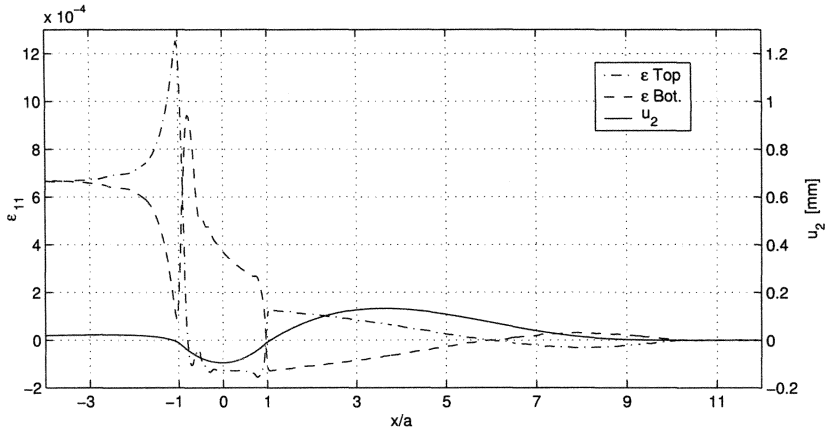

Figure 8: Tensile strain ϵ_{11} at the top and bottom surface of the first layer (dashed-dotted and dashed lines, respectively) and the vertical deflection u_2 of the center line of the top sheet (solid line). The nip is located in the range $-1 \leq x/a \leq 1$.

Within the first slip zone, in the vicinity of the nip front edge, the second layer is faster than the first one, the center part of the contact sticks and in the back of the nip the upper layer is faster. At the very end of the nip and behind the nip the lower sheet may be faster again. Note the difference in the speed behaviour of the drum-first layer contact as compared to the contacts between the layers below.

COMPARISON OF THE LAYERED AND SOLID MODELS

Since the mathematical model for a layered structure is computationally heavy, it would be beneficial if results of the same kind could be obtained or at least to some extent estimated using a solid model. For this reason the simulation of the previous section was repeated with the exception that a solid block, instead of a layered stack, under the nip was used. The calculated contact shear stresses at the top and bottom surfaces of each layer in the stack and the stresses at the corresponding locations of the solid block are shown in Fig. 9. As can be seen in Fig. 9(a) the stress distributions in the layered and solid models are considerably different. In the contact between the top surface and the drum both the layered and solid models display a slip zone at the beginning of the nip. The shear stress distributions in this region are qualitatively similar although the stress values and the size of the slip zone are larger in the solid. Behind this slip zone both contacts stick, the curves bend strongly and the stresses change sign before the center of the nip. The most dramatic difference occurs at the rear of the nip: the shear stress on the top of the solid remains negative throughout the latter part of the nip[2] whereas that on the top of the first layer of the stack bends back to positive values. As discussed earlier, the top surface of the first layer is moving faster than the drum in this region. In the case of the solid, however, the shear stress is negative so that the drum is moving faster than the surface of the solid. As can be seen from Fig. 9,

[2]excluding a tiny region ($\approx 5\%$ of a) at the very end of the nip

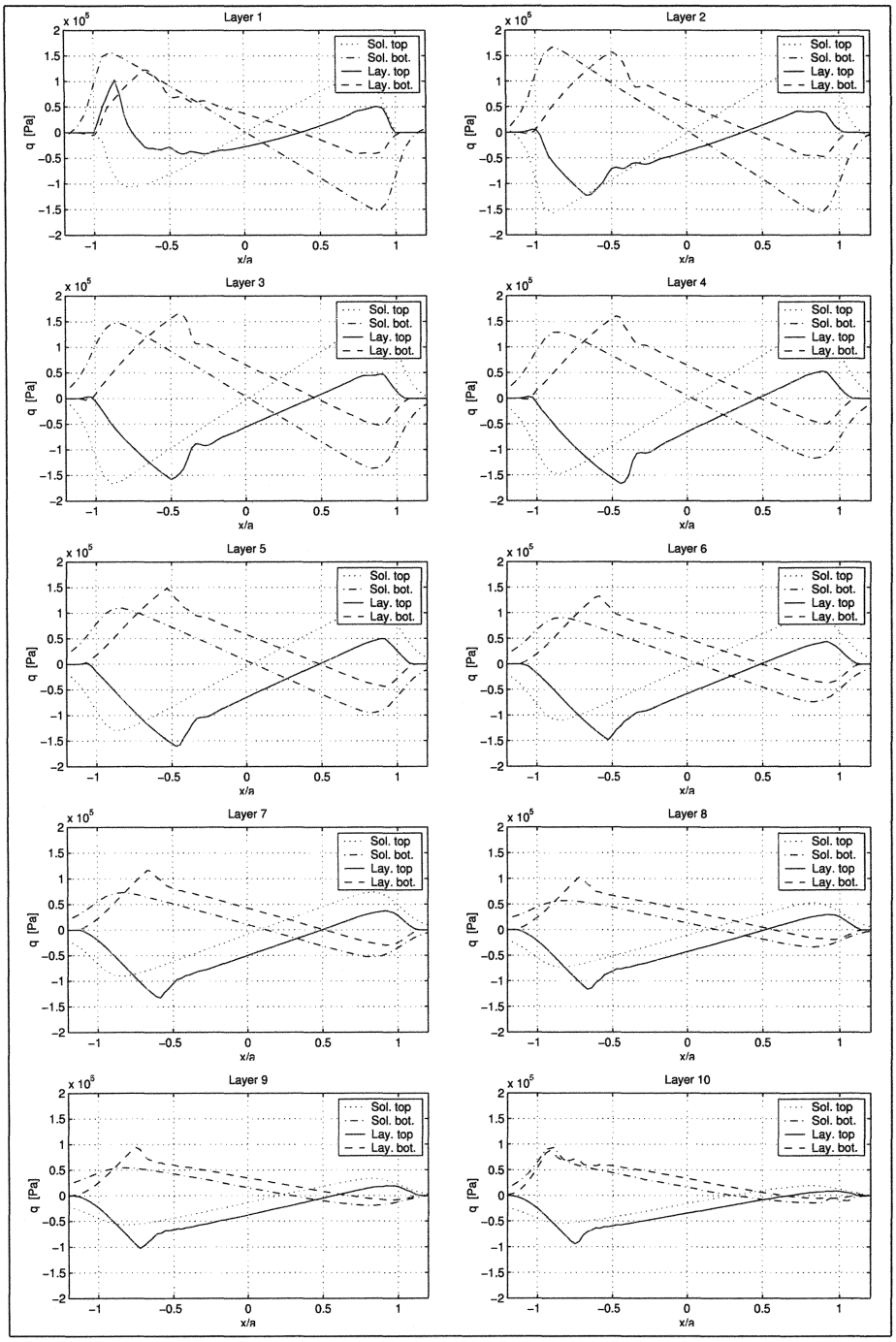

Figure 9: Shear stresses at the top and bottom surfaces of the layers in the stack (solid and dashed lines, respectively) and the corresponding stresses in the solid block (dotted and dashed-dotted lines).

the shear stress distributions of the solid are almost antisymmetric with respect to a vertical line through the center of the nip, i.e., the stresses in the right and left half of the nip are equal in magnitudes but to opposite directions. For this reason practically no net increase in the tensile stress is observed. It can also be seen that all the stresses are concentrated close to the nip area and are relieved soon behind the nip. In the layered case the contact pressure determines the upper limit for the shear stress between the layers ($q = \pm\mu p$). In the case of the solid this limitation is only present in the drum-solid and solid-bottom plate contacts. Consequently, the shear stresses in the solid are distributed to a wider area as can be seen in Fig. 9.

Figures 10(a) and (b) display the contour plots for the shear stress in the vicinity of the nip in the case of the layered and solid models, respectively. The

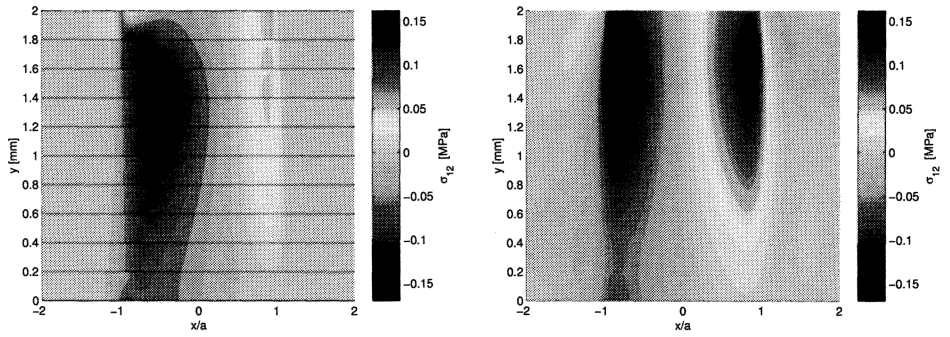

Figure 10: Shear stress distribution in the vicinity of the nip for the (a) layered model and (b) solid model.

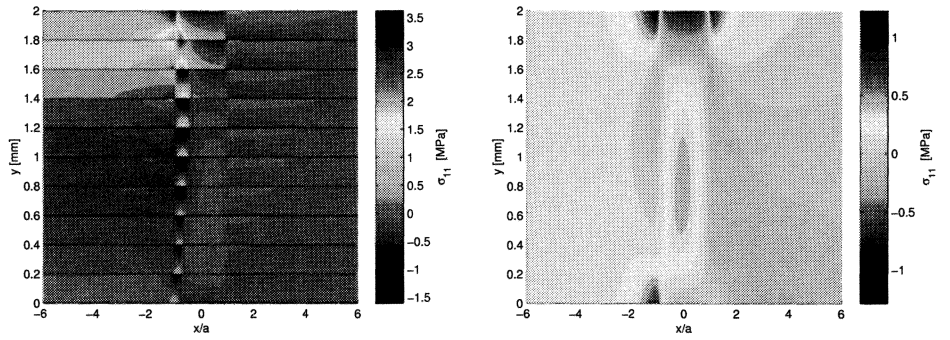

Figure 11: Lengthwise stress distribution in the vicinity of the nip for the (a) layered model and (b) solid model.

contour plots of Figs. 10 and 11 show the same information noted already earlier. The antisymmetry of the shear stress in the solid is clearly visible in Fig. 10(b). Because of the limited friction and the ensuing slippage between the layers in the layered model, the shear stress on the right side of the nip is considerably lower than in the solid. The bending of the individual sheets in front of the nip is clearly visible in Fig. 11(a).

CONCLUSIONS

A cylindrical steel drum rolling on a stack of separate paper sheets was studied. An exponential type saturation towards a limit value of the sheet tension of the top layers as the drum was rolled ahead was observed. The tensile stress at the bottom and surface of each layer could differ considerably in the nip area. This difference is mainly due to the bending of the sheet under the drum. The following observations on events taking place under the nip were made:

- Within about the first three quarters of the nip the contact shear stresses on the top and bottom surface of the first layer act in opposite directions and, thus, try to cancel each other. Near the trailing edge of the nip these contact shear stresses act *additively* in the same direction pointing towards the leading edge of the nip. Due to the balance of the sheet, this must be compensated for by a tensile stress in the sheet resulting in a significant tightening of the top layer.

- The contact shear stresses on the top and bottom surface of the other layers act always in opposite directions and partially cancel each other. The layers above the instant center experience a net tightening when passing the nip and those below the instant center a net slackening.

These basic phenomena for a stack of paper sheets are likely to be applicable to a wound roll as far as the topmost layers are concerned. The layers deeper in the roll, however, experience a cumulative normal stress due to the hoop tension of the layers above. This evidently leads to less slippage of these layers within the nip area. Consequently, the behaviour of the topmost layers obviously dominates when the nip-induced tension of a wound roll is considered.

REFERENCES

[1] Bentall, R. H. and Johnson, K. L., "An Elastic Strip in Plane Rolling Contact", Int. J. Mech. Sci., Vol. 10, 1968, pp. 637–663.

[2] Soong, T.-C. and Li, C., "The Steady Rolling Contact of Two Elastic Layer Bonded Cylinders With a Sheet in the Nip", Int. J. Mech. Sci., Vol. 23, 1981, pp. 263–273.

[3] Soong, T.-C. and Li, C., "The Rolling Contact of Two Elastic-Layer-Covered Cylinders Driving a Loaded Sheet in the Nip", J. Appl. Mech.-Trans. ASME, Vol. 48, Dec. 1981, pp. 889-894.

[4] Batra, R. C., "Rubber Covered Rolls – The Nonlinear Elastic Problem", J. Appl. Mech.-Trans. ASME, Vol. 47, March 1980, pp. 82–86.

[5] Hinge, K. C. and Maniatty, A. M., "Model of steady rolling contact between layered rolls with thin media in the nip", Engineering Computations, Vol. 15, No. 7, 1998, pp. 956–976.

[6] Kalker, J. J., "Viscoelastic Multilayered Cylinders Rolling With Dry Friction", J. Appl. Mech.-Trans. ASME, Vol. 58 , No. 3, 1991, pp. 666–679.

[7] Pfeiffer, J. D., "Mechanics of a Rolling Nip on Paper Webs", TAPPI Journal, Vol. 51, No. 8, Aug. 1968, pp. 77–85.

[8] Good, J. K. and Wu, Z., "The Mechanism of Nip-Induced Tension in Wound Rolls", J. Appl. Mech.-Trans. ASME, Vol. 60, Dec. 1993, pp. 942–947.

[9] McDonald, J. D. and Menard, A., "Layer-to-Layer Slippage Within Paper Rolls During Winding", J. Pulp. Pap. Sci., Vol. 25, No. 4, Apr. 1999, pp. 148–153.

[10] Jorkama, M., "Contact Mechanical Model for Winding Nip", Acta Polyt. Scan, Me 146, The Finnish Academies of Technology (2001)

[11] Jorkama M. and von Hertzen, R., "The Mechanism of Nip-Induced Tension in Winding", J. Pulp. Pap. Sci., Vol. 28, No. 8, Aug. 2002, pp. 280–284.

APPENDIX

The numerical values used in the calculation are given below.

Quantity	Value
General	
Number of paper layers	10
Thickness of one layer	0.2 mm
Number of elements in a layer (crosswise)	2
Length of paper layers	450 mm
Number of elements in a layer (lengthwise)	2399
Material	
Density	1000.0 kg/m^3
Elastic stiffness matrix	$E_{1111} = E_{3333} = 3000.0, E_{2222} = 20.0,$ $E_{1122} = E_{2233} = E_{1133} = 5.0,$ $E_{1212} = E_{1313} = E_{2323} = 10.0$ MPa
Drum	
Radius	250 mm
Rolling velocity v_{max}	0.5 m/s
Vertical displacement δ_{max}	0.1 mm
Friction coefficients	
drum-paper	0.3
paper-paper	0.2
paper-bottom plate	0.4
Other parameters	
Mass scaling factor	100.0
Duration of simulation	0.7 s
Acceleration due to gravity	10.0 m/s^2